




**Dissociative multiple ionization of carbon dioxide dimers in intense femtosecond laser fields**Pan Song,<sup>1</sup> Yalei Zhu,<sup>1</sup> Yan Yang,<sup>1</sup> Xiaowei Wang,<sup>1</sup> Congsen Meng,<sup>1</sup> Jing Zhao<sup>1</sup>,, Jinlei Liu<sup>1</sup>,, Zhihui Lv,<sup>1</sup> Dongwen Zhang,<sup>1</sup> Zengxiu Zhao,<sup>1,\*</sup> and Jianmin Yuan<sup>1,2,†</sup><sup>1</sup>*Department of Physics, National University of Defense Technology, Changsha 410073, China*<sup>2</sup>*Department of Physics, Graduate School of China Academy of Engineering Physics, Beijing 100193, China*

(Received 14 December 2021; revised 18 July 2022; accepted 2 August 2022; published 15 August 2022)

Molecular dimers have attracted much attention in the study of molecular structure and dynamics due to their complex interactions involving both weak van der Waals and strong covalent bonds. We investigate the dissociative ionization of carbon dioxide dimers exposed to intense femtosecond laser fields. The angular distributions of ionic fragments of the breakup channels  $(\text{CO}_2)_2^{2+} \rightarrow \text{CO}_2^+ + \text{CO}_2^+$  and  $(\text{CO}_2)_2^{3+} \rightarrow \text{CO}_2^{2+} + \text{CO}_2^+$  strongly depend on the laser intensity. Simulations based on time-dependent density-functional theory reproduce the experimental observations qualitatively and show that the angular distribution of fragments is determined by the angle-dependent orbital ionization probability and the relative contributions of different orbitals, both of which are intensity sensitive. By comparing the ionization of the dimer with  $\text{CO}_2$  monomer, we find that the weak van der Waals bond and molecular geometry in the dimer play considerable roles. This work extends significantly earlier studies of simple linear covalent bond molecules.

DOI: [10.1103/PhysRevA.106.023109](https://doi.org/10.1103/PhysRevA.106.023109)**I. INTRODUCTION**

Intricate ionization and dissociation occur when molecules are subjected to strong laser fields. With the presence of Coulomb repulsive force, photoinduced multiply-charged molecular ions are usually unstable and split up quickly into fragments with high kinetic energy [1–4]. Rich kinetic information of the molecular ionization has been obtained by studying the angular distribution of ionic fragments (ADIF). Among various contributing factors to the ADIF, both the geometric [5] and dynamic [6,7] alignment are found to be crucial. However, the mechanism of the anisotropic ADIF observed in complex molecules remains to be studied.

Double ionization of  $\text{CO}$ ,  $\text{CO}_2$ , and  $\text{C}_2\text{H}_2$  by few-cycle laser pulses with sufficiently low intensities [8] show that the first ionization steps are orientation dependent and determine the ADIF. The molecular tunneling ionization theory (MO-ADK) [9,10] implies that the symmetry of molecular orbitals determines the angular distribution of ionization probability. The dissociation of  $\text{O}_2$  and  $\text{N}_2$  with short laser pulses suggests that the ADIF is a direct indication of the angular ionization probability, which is related to the symmetry of the highest occupied molecular orbital (HOMO) [11]. In the case of long pulse or high laser intensity, the dynamic alignment mechanism plays a dominant role, where the laser-induced dipole moment aligns the molecular axis with the polarization direction of the laser. Therefore the ADIF peaks along the laser polarization direction. In addition to the well-known dynamic alignment of neutral molecules before ionization, postionization alignment of molecular ions has also been reported [12]. The dynamic alignment also allows molecule reorientation

during the dissociative multiphoton ionization [13]. However, the geometric alignment and dynamic alignment often coexist and are hard to be distinguished [14].

Molecules can form dimers through van der Waals (vdW) forces [15,16]. In comparison with covalently bonded molecules, dimers have longer internuclear distances. Dimers are ideal candidates for studying molecular dynamics, such as charge resonance enhanced ionization [17,18], interatomic Coulombic decay [19,20], intermolecular Coulombic decay [21], and radiative charge transfer [22,23]. The anisotropic ADIF observed in dissociative ionization of Ar dimers [24] was attributed to the angle-dependent enhanced ionization, and the angular distribution varied with laser intensity. Furthermore, field-driven electron transfer between the two atoms in an Ar dimer was found capable of triggering subcycle dynamics in neighboring atoms [25]. The structure and orientation of dimers govern the ionization dynamics [26–28] and the ADIF. The dissociation of  $\text{H}_2^+$  was found to be strongly aligned with the electric field [29], providing a natural frame in which the attoclock offset angle of  $\text{H}_2^+$  can be determined.

In this work, the dissociative double- and triple-ionization dynamics of  $(\text{CO}_2)_2$  driven by intense femtosecond laser pulses are investigated. The ADIFs in the breakup channels  $(\text{CO}_2)_2^{2+} \rightarrow \text{CO}_2^+ + \text{CO}_2^+$  and  $(\text{CO}_2)_2^{3+} \rightarrow \text{CO}_2^{2+} + \text{CO}_2^+$  are found anisotropic and change with laser intensity. Simulations based on time-dependent density functional theory (TDDFT) reproduce the experimental observations qualitatively and suggest that the isotropic ADIF arises from the angle-dependent electron orbital ionization probability and the involvement of multiple orbitals. In spite of its weak force, the vdW bond plays a considerable role in strong-field ionization. This work provides valuable insights into the strong-field ionization and dissociation dynamics of complex molecules.

\*zhaozengxiu@nudt.edu.cn

†jmyuan@nudt.edu.cn; jmyuan@giscaep.ac.cn

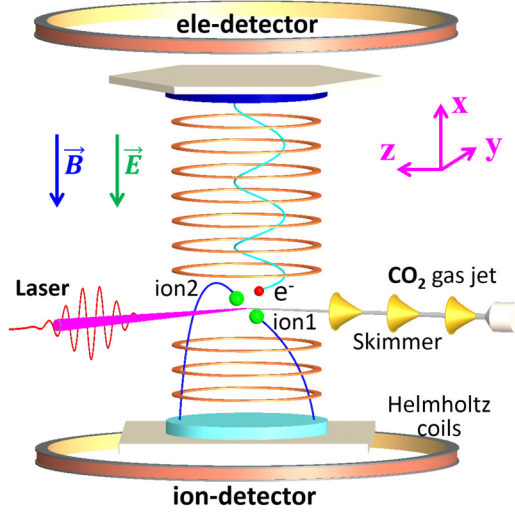


FIG. 1. Schematic drawing of the experimental setup. Strong laser pulses propagating along the  $y$  axis with polarization direction along the  $x$  axis are focused onto the  $(\text{CO}_2)_2$  beam from a nozzle located in the  $z$  axis. The fragmental ions and electrons were collected by the lower- and upper-position-sensitive delay line detector, respectively.

## II. EXPERIMENT

In the experiments,  $\text{CO}_2$  dimer are produced during the supersonic expansion of  $\text{CO}_2$  gas from a  $30\text{-}\mu\text{m}$  nozzle with 10-bar backing pressure. Only parallel-slipped structure of the carbon dioxide dimer was observed in the adiabatic expansion of the ultrasonic molecular beam [16,30–33]. The molecular beam passes through a three-stage vacuum differential pumping system to keep the background pressure below  $5 \times 10^{-10}$  mbar in the interaction chamber. The molecular beam is then crossed by a focused laser pulse with 25-fs pulse duration, 10-kHz repetition rate, and 790-nm central wavelength, as shown in Fig. 1. The laser peak intensity ranges from  $2 \times 10^{14}$   $\text{W}/\text{cm}^2$  to  $8.6 \times 10^{14}$   $\text{W}/\text{cm}^2$ . The ADIF is measured with a cold-target recoil-ion momentum spectrometer (COLTRIMS) [27,34], in which the ionic fragments and electrons are confined and guided by a uniform electric field and magnetic field before they reach the position-sensitive delay line detectors. The time of flight (TOF) and position of the charged particles are recorded to reconstruct their three-dimensional momenta. The momentum resolution for ion and electron detection can be as good as 0.05 a.u. and 0.02 a.u., respectively [35,36]. Depending on the channels to be analyzed, COLTRIMS can select events with two or more charged particles of photoions (photoion-photoion), photoelectrons (photoelectron-photoelectron), or both of them (photoion-photoelectron). The  $x$ ,  $y$ , and  $z$  axis of the laboratory coordinate system are defined as the direction of laser polarization, laser propagation, and molecular beam, respectively, as shown in Fig. 1.

The dissociative double-ionization channel  $(\text{CO}_2)_2^{2+} \rightarrow \text{CO}_2^+ + \text{CO}_2^+$  and triple-ionization channel  $(\text{CO}_2)_2^{3+} \rightarrow \text{CO}_2^{2+} + \text{CO}_2^+$  are analyzed and hereafter denoted as  $(\text{CO}_2)_2[1, 1]$  and  $(\text{CO}_2)_2[2, 1]$ , respectively. To reduce the possible pollution from other fragmentation channels to the

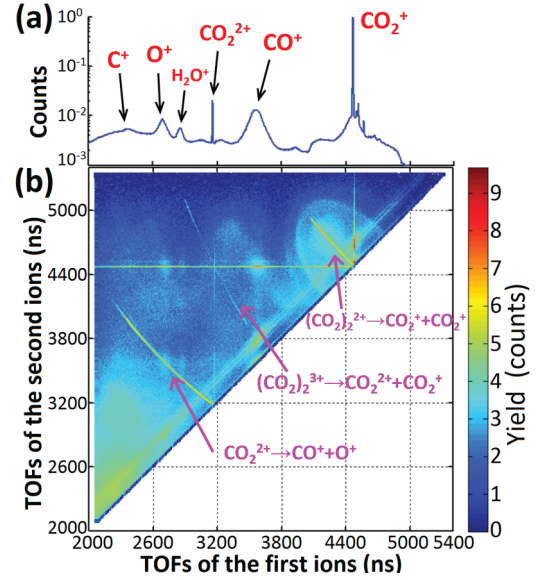


FIG. 2. (a) TOF spectrum of supersonic  $\text{CO}_2$  gas beam irradiated by 790-nm, 25-fs linearly polarized laser pulses of intensity  $4 \times 10^{14}$   $\text{W}/\text{cm}^2$  and (b) PIPICO spectrum. Three breakup channels are identified.

authenticity of the coincidence measurement, the experimental data are filtered with three conditions: (1) only two  $\text{CO}_2^+$  ions are collected from each event for the  $(\text{CO}_2)_2[1, 1]$  channel, and only one  $\text{CO}_2^{2+}$  ion and one  $\text{CO}_2^+$  ion are collected from each event for the  $(\text{CO}_2)_2[2, 1]$  channel; (2) the sum of their momenta is small enough to fulfill momentum conservation, i.e.,  $\sum P_z < 10$  a.u.,  $\sum P_y < 4.5$  a.u., and  $\sum P_x < 2.5$  a.u.; (3) their relative momenta is large enough to rule out false coincidences, i.e.,  $|\mathbf{P}(\text{CO}_2^+) - \mathbf{P}(\text{CO}_2^+)| > 100$  a.u. and  $|\mathbf{P}(\text{CO}_2^{2+}) - \mathbf{P}(\text{CO}_2^+)| > 100$  a.u..

## III. RESULTS AND DISCUSSION

In the TOF spectrum of the supersonic  $\text{CO}_2$  gas beam ionized by laser pulses with intensity of  $4 \times 10^{14}$   $\text{W}/\text{cm}^2$  as shown in Fig. 2(a), fragmental ions of  $\text{CO}_2^+$ ,  $\text{CO}_2^{2+}$ ,  $\text{CO}^+$ ,  $\text{O}^+$ , and  $\text{H}_2\text{O}^+$  are identified. Figure 2(b) shows the photoion-photoion coincidence (PIPICO) spectrum. The back-slant line structures in the PIPICO spectrum represent different Coulomb explosion channels. All the other events, such as the horizontal and vertical lines, and the arc structure around the  $(\text{CO}_2)_2[1, 1]$  channel, are false coincidences. With the filtering conditions mentioned above, ionic fragments for the two breakup channels  $(\text{CO}_2)_2[1, 1]$  and  $(\text{CO}_2)_2[2, 1]$  are picked out.

### A. Dissociative double and triple ionization

Dissociative double ionization of  $(\text{CO}_2)_2$  is investigated under three different laser intensities:  $I_0 = 2 \times 10^{14}$   $\text{W}/\text{cm}^2$ ,  $2I_0$  and  $4I_0$ , whereas three higher intensities ( $2I_0$ ,  $2.8I_0$ , and  $4.3I_0$ ) are used for dissociative triple ionization. For the  $(\text{CO}_2)_2[1, 1]$  channel, the kinetic energy release (KER) spectra shown in Fig. 3(a) have a unique, constant peak at 3.8 eV for all three laser intensities. The same behavior is

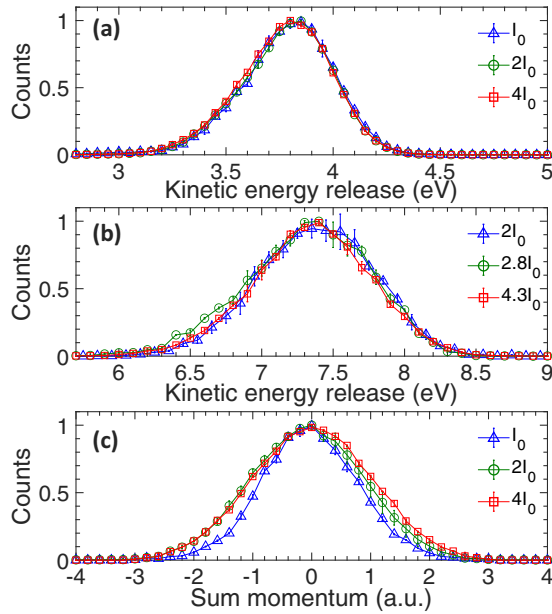


FIG. 3. The KER for the dissociative channels  $(\text{CO}_2)_2[1, 1]$  (a) and  $(\text{CO}_2)_2[2, 1]$  (b). The KER maximizes at the same energy of 3.8 eV for the  $(\text{CO}_2)_2[1, 1]$  channel under laser intensities of  $I_0$  (triangles),  $2I_0$  (circles), and  $4I_0$  (squares);  $(\text{CO}_2)_2[2, 1]$  channel has 7.4-eV KER for laser intensities of  $2I_0$  (triangles),  $2.8I_0$  (circles), and  $4.3I_0$  (squares). (c) The ion pair sum-momentum distributions along the direction of laser polarization for the dissociative channels  $(\text{CO}_2)_2[1, 1]$  under laser intensities of  $I_0$  (triangles),  $2I_0$  (circles), and  $4I_0$  (squares).

observed for KER spectra of  $(\text{CO}_2)_2[2, 1]$  channel shown in Fig. 3(b) but with peak position at 7.4 eV. For the dissociative double-ionization channel  $(\text{CO}_2)_2[1, 1]$ , the fragments can result from two competing double-ionization processes: two-site double ionization and one-site double ionization. Two-site double ionization is also called the direct double-ionization process, wherein one electron is removed from each molecule of the dimer. For one-site double ionization, two electrons are removed from one site of the dimer first, populating the  $\text{CO}_2^{2+} - \text{CO}_2$  nondissociative molecular state [37], and then this transient state can further relax to the same dissociative states as in the two-site double ionization through radiative charge transfer (RCT). The RCT process happens at a smaller internuclear distance than the equilibrium distance of the dimer, resulting in a higher KER than the energy expected for the direct double-ionization process [37–39]. As shown in Figs. 3(a) and 3(b), the single-peak structure in KERs distribution indicates that each of the two breakup channels has one definite ionic state for different laser intensities [40]. With approximate Coulomb potential  $E = 1/R$ , the vdW bond length of laser-produced  $(\text{CO}_2)_2^{2+}$  and  $(\text{CO}_2)_2^{3+}$  ions are determined to be 3.79 Å and 3.89 Å, respectively, which are close to the ground-state bond lengths 3.6 Å of the  $(\text{CO}_2)_2$  [16,27,30]. Therefore the RCT process can be eliminated, and only two-site double ionization should be considered in our experiments. For a triple ionization channel, it can be determined that one  $\text{CO}_2$  molecule is doubly ionized and the other one is singly ionized based on the same analysis.

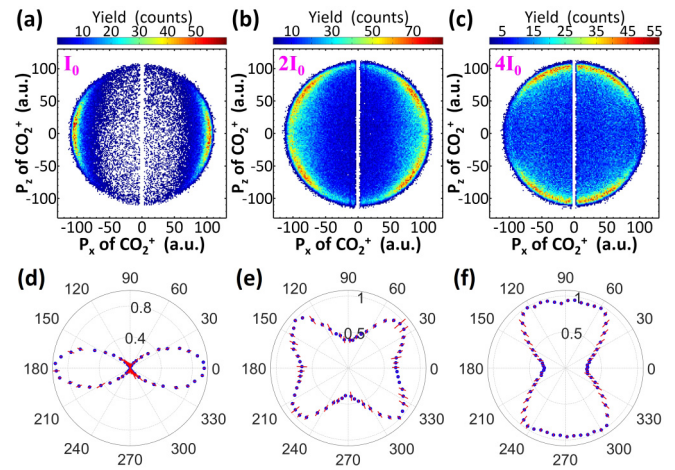


FIG. 4. The projections of the 3D momenta of  $\text{CO}_2^+$  in the  $(\text{CO}_2)_2[1, 1]$  channel onto the  $xz$  plane of the laboratory frame for laser intensities of  $I_0$  (a),  $2I_0$  (b), and  $4I_0$  (c). The angular distribution of ionic fragments for  $I_0$  (d),  $2I_0$  (e), and  $4I_0$  (f), where the laser polarization vector is horizontal.

It is well known that there are two mechanisms for double ionization, i.e., sequential double ionization (SDI) and non-sequential double ionization (NSDI) [7]. In general, NSDI and SDI dominates for low and high intensity, respectively. Nevertheless, the exact laser intensity for the transition from NSDI to SDI also depends on the gas species [41–43]. Figure 3(c) shows the distribution of sum momentum of the  $\text{CO}_2^+/\text{CO}_2^+$  ion pair in the direction of laser polarization for laser intensity of  $I_0$  (triangles),  $2I_0$  (circles), and  $4I_0$  (squares), respectively. The Gaussian-like structure with only one peak indicates SDI as the main mechanism of the present two-site double ionization of  $\text{CO}_2$  dimer, since NSDI would result in a “double-hump” structure [38,44,45]. There is more momentum broadening in the  $2I_0$  and  $4I_0$  curves than the  $I_0$  curve in Fig. 3(c). The greater momentum broadening for the higher laser intensity is likely caused by the rescattering-induced NSDI, when the laser field direction has a large angle to the vdW bond. Normally, the rescattering-induced NSDI is expected to be more apparent at lower laser intensity  $I_0$ . However, in the following it will be seen that at  $I_0$  the ionizations are mainly produced when the laser field is along the vdW bond, so that the rescattering-induced two-site double ionization may be blocked by the Coulomb scattering of the ionized  $\text{CO}_2^+$  ion, because the  $\text{CO}_2^+$  ion is in the way of the turn back electron to impact the  $\text{CO}_2$  molecule at the other side of the dimer and the Coulomb potential can strongly change the trajectory of the incident electron.

In addition to KER spectra, the three-dimensional (3D) momenta of ionic fragments and electrons are retrieved in the coincidence measurements. For the  $(\text{CO}_2)_2[1, 1]$  channel, the projections of the 3D momenta of  $\text{CO}_2^+$  onto the  $xy$  plane of the laboratory frame are shown in Figs. 4(a), 4(b) and 4(c) for laser intensities of  $I_0$ ,  $2I_0$ , and  $4I_0$ , respectively. The vertical blank in these figures is artificial due to the dead time of the ion detector. Figures 4(d), 4(e) and 4(f) show the angular distributions of the ion pair  $\text{CO}_2^+/\text{CO}_2^+$  generated from the channel of  $(\text{CO}_2)_2[1, 1]$  under laser intensities of  $I_0$ ,



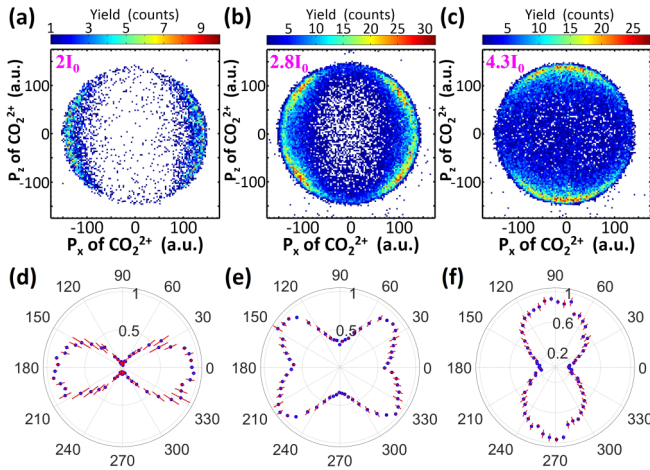


FIG. 5. The projections of the 3D momenta of  $\text{CO}_2^{2+}$  in  $(\text{CO}_2)_2[2, 1]$  channel onto the  $xz$  plane of the laboratory frame for laser intensities of  $2I_0$  (a),  $2.8I_0$  (b), and  $4.3I_0$  (c). The angular distribution of ionic fragments for  $2I_0$  (d),  $2.8I_0$  (e), and  $4.3I_0$  (f), where the laser polarization vector is horizontal.

$2I_0$ , and  $4I_0$ , respectively. Evidently, the ADIFs are anisotropic and change with laser intensity. With low laser intensity, the fragmental ions exhibit strongly uniaxial anisotropic angular distribution with major axis aligned with the laser polarization. As laser intensity increases, the major axis of anisotropic ADIF gradually becomes perpendicular to the laser polarization direction.

The projections of the 3D momenta of  $\text{CO}_2^{2+}$  in the  $(\text{CO}_2)_2[2, 1]$  channel onto the  $xz$  plane are shown in Figs. 5(a), 5(b) and 5(c) for laser intensities of  $2I_0$ ,  $2.8I_0$ , and  $4.3I_0$ , respectively. Figures 5(d), 5(e) and 5(f) show the angular distributions of the ion pair  $\text{CO}_2^+/\text{CO}_2^+$  generated from the channel of  $(\text{CO}_2)_2[1, 1]$  under laser intensities of  $I_0$ ,  $2I_0$ , and  $4I_0$ , respectively. Despite the lower yields and poorer signal-to-noise ratio, the angular distribution is almost identical to that of  $\text{CO}_2^+$  fragments in the double-ionization channel. Note that the two fragments are different in the  $(\text{CO}_2)_2[2, 1]$  channel, and the detector dead times do not cause any problems here. The ADIFs are shown in Figs. 5(d), 5(e) and 5(f), corresponding to laser intensities of  $2I_0$ ,  $2.8I_0$ , and  $4.3I_0$ , respectively. The ADIFs of the  $(\text{CO}_2)_2[2, 1]$  channel also exhibit significant modulation with increasing laser intensity. The triple ionization of carbon dioxide dimer is to ionize one more electron on the basis of double ionization, and doubly charged molecules are almost certainly the precursors of all higher charged molecules [7]. In the triple ionization of carbon dioxide dimer, the  $\text{CO}_2^{2+}$  ion is produced by a double ionization occurring on the same side of the dimer, in which the rescattering-induced NSDI on the same side may contribute more without a Coulomb potential scattering in advance. The end result is one  $\text{CO}_2$  molecule is doubly ionized and the other one is singly ionized  $\text{CO}_2^{2+} - \text{CO}_2^+$ , leading to angular distributions similar to the  $\text{CO}_2^+ - \text{CO}_2^+$  dissociation channel but at higher laser intensities because of the difficulty to ionize one more electron. Thus an understanding of the mechanisms for dissociative double ionization stands the possibility of helping considerably in unravelling

the dissociative triple-ionization process. In the following discussion, we will analyze the reason why the fragment ion angle distribution changes with the laser intensity during the double-ionization process.

### B. Orientation-dependent strong-field ionization of a dimer

In intense femtosecond laser fields, molecules exhibit abundant nonlinear characteristics. For certain internuclear distances, charge-resonance-enhanced ionization [18,46–49] occurs. Previous studies have shown that odd-charged ions have a critical internuclear distance for the occurrence of Coulomb explosion, and the ionization rate of triatomic ions can be strongly enhanced by stretching one or both of its bonds to a critical distance [17]. In particular, these phenomena are only observed when the molecular axis is parallel to the laser polarization, and the enhanced ionization probability changes as laser polarization rotates around the molecular axis, resulting in anisotropic ADIF. For vdW clusters, in addition to the geometric structure, the orientation of the different chemical bonds with respect to the laser polarization also matters in the ionization dynamics. It is found that the breakup of the vdW bond in strong-field ionization of  $\text{N}_2\text{Ar}$  is favored when it is aligned along the laser polarization for both dissociative double and triple ionizations [26]. The orientation of the covalent bond governs triple ionization when both the covalent and vdW bonds break at the same time. The carbon dioxide dimer contains both covalent bonds and vdW bonds, which makes it a perfect candidate to study the orientation-dependent strong-field ionization of chemical bonds with different properties. The photoelectron momentum and angular distribution produced during double ionization may help to shed light on the roles which the orientation and properties of chemical bonds of the  $(\text{CO}_2)_2$  play during dissociative ionization.

Together with the ADIF, which indicates the geometric structure of the dimer, the angular distribution of photoelectrons reveals the ionization dynamics. In the experiments we use high-resolution coincidence techniques in which the momentum of  $\text{CO}_2^+ + \text{CO}_2^+$  and one electron are recorded with COLTRIMS. We did not measure the momenta of both electrons due to the low electron detection efficiency and detector dead time. The angular distribution of electron momentum with respect to the laser polarization is then plotted in Fig. 6(a) for laser intensity of  $I_0$  (blue line with circular markers) and  $4I_0$  (red line with diamond markers). The photoelectrons are mainly emitted along  $0^\circ$  and  $180^\circ$  for both intensities, i.e., along the polarization direction of the laser field, which is consistent with the tunneling ionization theory. To investigate the ionization dynamics in the molecular frame, the angular distribution of electron momentum with respect to the vdW bond of the dimer is shown in Fig. 6(b). The direction of the vdW bond is defined as the direction of  $\mathbf{P}_1 - \mathbf{P}_2$ , where  $\mathbf{P}_1$  and  $\mathbf{P}_2$  are the momentum of first and second ion fragments. With lower laser intensity, there are two peaks at around  $0^\circ$  and  $180^\circ$ , as shown by the blue line with circle markers in Fig. 6(b), i.e., the photoelectrons are mainly emitted along the vdW bond of the dimer. Therefore the dimers with vdW bonds aligned with laser polarization, as illustrated in Fig. 6(c), are favored by double ionization. As laser intensity increases up to

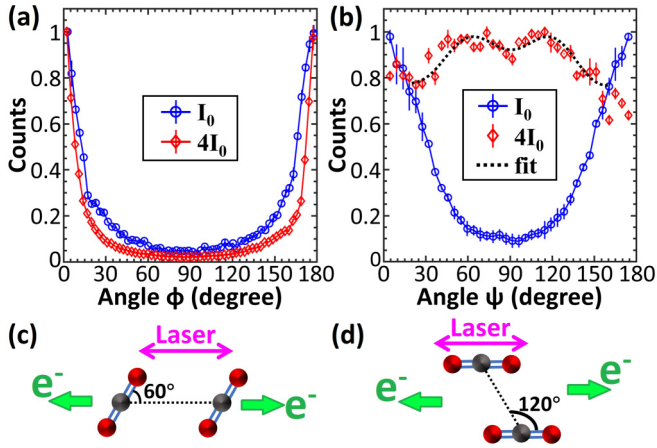


FIG. 6. (a) The angular distribution of electron momentum with respect to the laser polarization for laser intensity of  $I_0$  (blue line with circle markers) and  $4I_0$  (red line with diamond markers); (b) the angular distribution of electron momentum with respect to the vdW bond of the dimer for laser intensity of  $I_0$  (blue line with circle markers) and  $4I_0$  (red diamond markers), the black dashed curves is the smooth fitting of data. The electron angular distributions are shown for the  $\text{CO}_2^+ + \text{CO}_2^+$  breakup channel and the solid detection angle bias has been taken into account during the calculation of the angle in (a) and (b) by dividing the yield with  $\sin(\Psi)$ . The angular schematic diagram of electron emission direction with respect to the vdW bond of the dimer for laser intensity  $I_0$  (c) and  $4I_0$  (d).

$4I_0$ , the angular distribution becomes more isotropic, with two wide peaks around  $60^\circ$  and  $120^\circ$  as shown by the red diamond markers in Fig. 6(b); the black dashed curves are the Gaussian distributions of the fit. The angle between the  $\text{O}=\text{C}=\text{O}$  bond and vdW bond happens to be  $60^\circ/120^\circ$ . Therefore the electrons emitted along the  $\text{O}=\text{C}=\text{O}$  bond of the dimer may produce these two broad peaks. According to Fig. 6(a), the electron emission direction is parallel to the laser polarization, so the dimers whose  $\text{O}=\text{C}=\text{O}$  covalent bonds are parallel to the laser polarization, as illustrated in Fig. 6(d), have maximal double-ionization probability. However, the overall angular distribution is roughly isotropic, indicating that the ionization anisotropy of photoelectrons is weakened under high laser intensity.

The experimental results directly show that the orientation of the vdW and covalent bonds relative to the laser polarization affects the dissociative multi-ionization dynamics of the dimer. With low laser intensities, the ionization probability reaches a relatively sharp maximum when the vdW bond is parallel to the laser polarization. The ionic fragments show an anisotropic angular distribution with the peak along the laser polarization axis, as shown in Fig. 4(d). With high laser intensities, the dimer ionization probability displays two broad bumps corresponding to the emission of covalent bond direction, that is, the ionization probability reaches a maximum when the covalent bond orientation is along the laser polarization, leading to the angular distribution of fragmental ions generated by dimer dissociation deviating from the laser polarization direction, as shown in Fig. 4(f). Therefore the ADIF of  $(\text{CO}_2)_2$  shows rich modulation phenomena as the laser intensity changes, which indicates that dimers with

specific orientation are selectively ionized under different laser intensities.

### C. Multiorbital ionization of carbon dioxide dimer

The shape of the molecular orbitals is well known to have a great influence on ionization probability. Both MO-ADK [9] and the strong-field approximation calculation [50] predict that the single-ionization rate depends strongly on the angle between the electric field and the molecular axis. Moreover, the MO-ADK theory explains well the ionization suppression of some molecules. The shape and symmetry of molecular orbitals are found to play important roles in strong-field ionization [10,51–53]. The ionization probability of  $\text{N}_2$  is found to be about four times greater for molecules aligned to the laser field than that for molecules antialigned to the laser field [54]. The same phenomenon was reported [55] for CO molecules with a twofold increase in ionization probability. The geometric structure of CO orbitals is considered a dominant factor in strong-field tunneling ionization [56], and the influence of the linear Stark effect of the orbital dipole plays a secondary role. In addition to the HOMO, inner molecular orbitals substantially contribute to the total ionization probability [57]. Recent studies have shown that molecular electronic states with energy lower than the HOMO contributes to high harmonic generation (HHG), and the contributions of multichannels in HHG have been widely studied [58–60]. Moreover, the coherent HHG emission from multiple channels can resolve the multielectron dynamics effectively and provide a snapshot of the structure and dynamics of the molecular system.

To understand the intensity dependence of dissociative double and triple ionizations of  $(\text{CO}_2)_2$ , we study the electronic dynamics with TDDFT. The calculations are carried out with the OCTOPUS package [61]. According to previous work, we choose the modified Leeuwen-Baerends  $\text{LB}\alpha$  potential function as the exchange-correlation core function [62] and employ the Troullier-Martines pseudopotential to fix the  $1s^2$  electrons of C and O. The electron density at position  $\mathbf{r}$  is described by  $\rho(\mathbf{r})$ . The  $\text{LB}\alpha$  function,

$$v_{xc}^{\text{LB}\alpha}(\alpha, \beta, \mathbf{r}) = \alpha v_x^{\text{LDA}}(\mathbf{r}) + v_c^{\text{LDA}}(\mathbf{r}) - \frac{\beta x^2(\mathbf{r}) \rho^{1/3}(\mathbf{r})}{1 + 3\beta x(\mathbf{r}) \ln\{x(\mathbf{r}) + [x^2(\mathbf{r}) + 1]^{1/2}\}}, \quad (1)$$

$$x(\mathbf{r}) = \frac{|\nabla \rho(\mathbf{r})|}{\rho^{4/3}(\mathbf{r})}, \quad (2)$$

describes the long-range Coulombic potential. The parameters are set as  $\alpha = 1.25$  and  $\beta = 0.01$  to fit the experimental data of the  $\text{CO}_2$  molecular orbitals [62]. The  $(\text{CO}_2)_2$  has 32 active electrons occupying 16 orbitals. The projections of the 12 static ground-state orbital wave functions on the  $xz$  plane are shown in Fig. 7. The orbitals of the  $(\text{CO}_2)_2$  exhibit nondegenerate features due to the vdW bond, which results in significant orbital deformation in both HOMO and HOMO-1 orbitals. These deformed orbitals of the dimer respond differently during ionization compared to that of the monomer. By subjecting the dimer to intense laser fields, the temporal evolution of the electron density is calculated, and the ionization probability is evaluated until the laser pulse

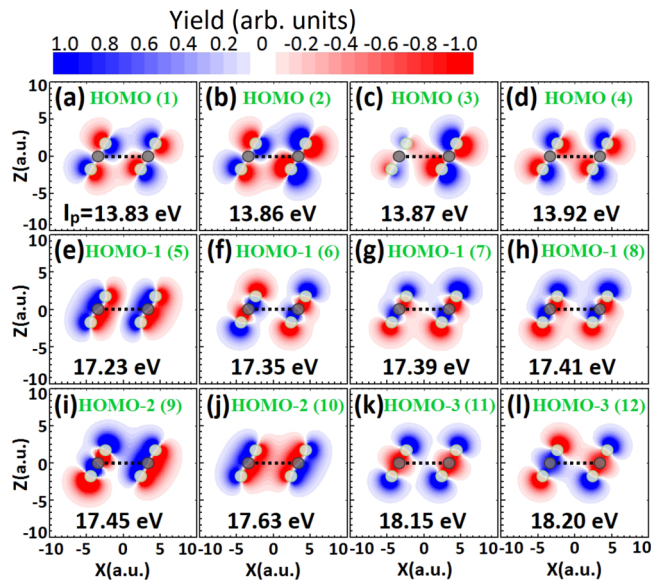


FIG. 7. Projections of the 12 static ground-state orbital wave functions of a  $(\text{CO}_2)_2$  on the  $xz$  plane. From (a) to (l), the ionization energies from their ground state progressively increase: (a, b, c, d) show four HOMO orbitals, (e, f, g, h) show four HOMO-1 orbitals, (i, j) show two HOMO-2 orbitals, and (k, l) show two HOMO-3 orbitals.

vanishes. The ionization contribution of orbital  $n$  is defined as  $\bar{P}_n = 1 - P_n$ , where  $P_n$  is the population of ground orbital  $n$  after the laser. The identification of approximate  $k$  ionization probability  $P^k$  is from Ref. [63].

Figure 8 presents the results from TDDFT calculations of the double-ionization probabilities of  $(\text{CO}_2)_2$  as a function of the angle  $\theta$  between laser polarization and the vdW bond with laser intensity of  $I_0$  (green solid line),  $2I_0$  (red dotted line), and  $4I_0$  (blue dotted dash line). Only two special cases are taken into account, as shown in Figs. 8(a) and 8(b), i.e., the laser polarization is in the first plane defined by the  $\text{O}=\text{C}=\text{O}$  and vdW bonds (case 1), and the laser polarization is in the second plane, which is perpendicular to the first plane but containing the vdW bond in it (case 2). The double-ionization probabilities of  $(\text{CO}_2)_2$  for case 1, case 2, and their summation are shown in Figs. 8(d), 8(e) and 8(f), respectively. Note that since the  $(\text{CO}_2)_2$  is not axisymmetric, experimental measurements cannot identify the positive and negative orientation of the molecular axis. We introduce a symmetry along the axis in theoretical calculations for a comparison with experimental results as shown in Fig. 8(f). The double-ionization probabilities show significant anisotropic features. The ionization probability is the highest when the vdW bond of the dimer is parallel to the laser polarization for low laser intensities. However, with increasing laser intensity, the ionization probability around the vertical direction rises steeply and even exceeds that for the horizontal direction. This agrees with our experimental results, indicating that the ADIF is determined by the ionization process.

In two-site double ionization of the  $(\text{CO}_2)_2$ , each electron is liberated from one  $\text{CO}_2$  site, so it might have a similar angular distribution to the  $\text{CO}_2$  monomer, if the electronic orbitals were not significantly changed by the vdW bond and

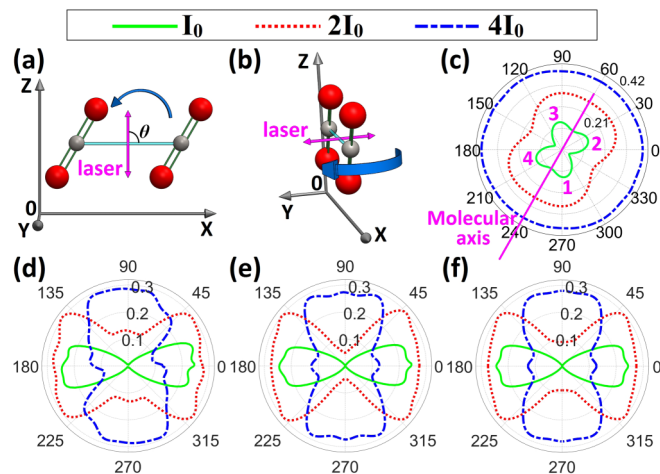


FIG. 8. Ionization probabilities of  $(\text{CO}_2)_2$  for different angles  $\theta$  between laser polarization and vdW bond with laser intensity of  $I_0$  (green solid line),  $2I_0$  (red dotted line), and  $4I_0$  (blue dotted dash line) calculated with TDDFT. We take into account only two special cases, (a) the laser polarization is in the first plane defined by  $\text{O}=\text{C}=\text{O}$  and the vdW bond for case 1, and (b) the laser polarization is in the second plane, which is perpendicular to the first plane but containing the vdW bond in it, for case 2. (c) The single-ionization probability of  $\text{CO}_2$  monomer as a function of the angle  $\theta$  between laser polarization and the  $\text{O}=\text{C}=\text{O}$  bond. We rotated the results by  $60^\circ$  counterclockwise for comparison with dimers, and the axis along the  $\text{O}=\text{C}=\text{O}$  bond is illustrated. The ionization probabilities with laser intensity of  $I_0$  are scaled by a factor of 2 for better visibility. The double-ionization probabilities of  $(\text{CO}_2)_2$  for case 1 (d) and case 2 (e) and their summation (f). Here the results in (f) are artificially symmetrized, since molecules are not orientated in the experiments.

the molecular geometry in the dimer did not play a role. Figure 8(c) shows the single-ionization probability of the  $\text{CO}_2$  monomer, the angle  $\theta$  between the laser polarization and the  $\text{O}=\text{C}=\text{O}$  bond. We rotated the results by  $60^\circ$  counterclockwise for comparison with the dimers. The axis along the  $\text{O}=\text{C}=\text{O}$  bond is illustrated in Fig. 8(c). With low light intensities, the distribution has a butterfly shape with four peaks labeled 1–4. As the laser intensity increases, the distribution gradually becomes isotropic, which may be attributed to the barrier ionization under high laser intensity. The ionization probability of the dimer is quite different from that of the  $\text{CO}_2$  molecule. With the lowest light intensity, peaks 2 and 4 of the butterfly-shaped distribution shown in Fig. 8(c) are enhanced significantly, resulting in an extremely anisotropic strong ionization along the vdW bond. As laser intensity increases from  $I_0$  to  $4I_0$ , the anisotropy changes its features along with the laser intensity changes but is still significant compared to the  $\text{CO}_2$  molecule. Interactions involving the vdW bonds are normally weak, but two-site  $\text{CO}_2$  dimer double ionization is thus not equivalent to the ionization of two independent monomer molecules. The vdW bonds change the ionization characteristics of the two  $\text{CO}_2$  monomers dramatically, and the  $\text{CO}_2$  dimer structure of the system matters.

To reveal the mechanism of the complex angular distribution, the ionization dynamics of different molecular orbitals need to be investigated. The strong anisotropic ionization



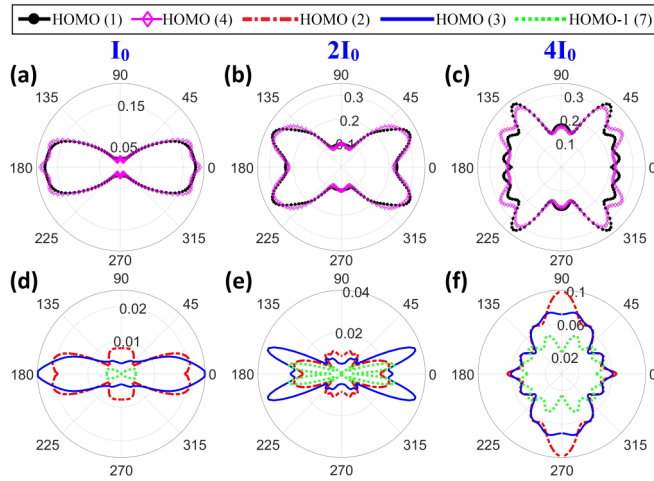


FIG. 9. Calculated angular ionization contribution for multi-orbital of carbon dioxide dimer. (a), (b), and (c) Calculated angular ionization contribution for HOMO-1 (black solid line with dotted marker) and HOMO-4 (carmine solid line with rhombus marker). The calculations are done with laser intensity of  $I_0$ ,  $2I_0$ , and  $4I_0$  for case 1. (d), (e), and (f) Calculated angular ionization contribution for HOMO-2 (red dotted and dash line), HOMO-3 (blue solid line), and HOMO-1 (7) (green dotted line). The calculations are done with laser intensity of  $I_0$ ,  $2I_0$ , and  $4I_0$  for case 1. Here, all diagrams are also artificially symmetrized.

probability for different orbitals of  $(\text{CO}_2)_2$  is shown in Fig. 9. The ionization probability of different orbitals versus  $\theta$  defined in Fig. 8(a) is calculated. Figures 9(a), 9(b) and 9(c) show the angular ionization probabilities of HOMO-1 and HOMO-4 orbitals for laser intensities of  $I_0$ ,  $2I_0$ , and  $4I_0$ , respectively, for case 1. Figures 9(d), 9(e) and 9(f) show the angular ionization probabilities of three orbitals for HOMO-2 (red dotted and dashed line), HOMO-3 (blue solid line), and HOMO-1 (7) (green dotted line). The calculations are done with laser intensity of  $I_0$ ,  $2I_0$ , and  $4I_0$  for case 1. As can be seen from the inset of Fig. 9, the angular ionization contribution of different orbitals changes with laser intensity, which inevitably affects the double-ionization probability of the dimer. The HOMO-1 (black solid line with dotted marker) and HOMO-4 (carmine solid line with rhombus marker) have a primary contribution that dominates the angular distribution at intensities  $I_0$  and  $2I_0$ . As laser intensity increases, the ionization probabilities of HOMO-2 (red dotted and dash line) and HOMO-3 (blue solid line) also change significantly. From the orbital resolved ionization shown in Fig. 9, it could be deduced that for the  $\text{CO}_2^{2+} + \text{CO}_2^+$  breakup in Fig. 5(f), after two electrons have been ionized from HOMO-1 and HOMO-4 orbitals, the third ionization from the orbitals HOMO-2 and HOMO-3 may contribute to produce a more strictly perpendicular orientation of the vdW axis with respect to the polarization for high intensity. The ionization of each orbital is modulated strongly by the molecular geometry of the dimer. The modulation depends on the intensity of the laser field in a way that matches the

critical interatomic distance between the two  $\text{CO}_2$  molecules in the dimer via the so-called charge-resonance-enhanced ionization [24,38,44]. When the laser pulse with proper intensity polarizes along a biatomic connection line between the two  $\text{CO}_2$  molecules in the dimer, the two-site double ionization of the connected biatomic system may be enhanced significantly due to the charge-resonance-enhanced ionization. This can be seen from the enhanced  $\text{CO}_2^+ + \text{CO}_2^+$  dissociation at  $I_0$  when the laser polarizes along the vdW bond from both experimental and TDDFT calculations shown in Fig. 4(d) and Figs. 8(d)–8(f). In addition, with the increase of light intensity, the ionization contribution of inner orbitals (such as HOMO-1) also increases; therefore the multi-orbital ionization of carbon dioxide dimer results in the variation of double-ionization probability with light intensity. As shown in Fig. 8(f), the ionization probability around the vertical direction rises steeply and even exceeds the parallel direction with increasing laser intensity, which can be ascribed to the contribution change of the multi-orbital. The results indicate that the angular distribution of fragmental ions is determined by the ionization process and related to multiple orbitals.

#### IV. CONCLUSION

We investigated the intensity dependence of dissociative multi-ionization of  $(\text{CO}_2)_2$  subjected to femtosecond laser fields. We show that the ADIF depends greatly on the laser intensity. The TDDFT simulations show that the ADIF is determined by the anisotropic ionization processes with contributions from multiple molecular orbitals. Moreover, for low laser intensities, the ionization of HOMO-1 and HOMO-4 plays a dominant role and shows a significant difference from that of the  $\text{CO}_2$  molecule due to the weak vdW bond. The relative contribution of HOMO-2 and HOMO-3, and the lower occupied orbitals HOMO-1 increases from about 10% to 30% and could come into play as laser intensity increases farther. On the other hand, dimer orientation with respect to the laser polarization alters the relative contribution from different orbitals. The geometric alignment mechanism results in maximum ionization probability along the vdW bond of the dimer for low laser intensity and maximum ionization probability along the direction of the  $\text{O}=\text{C}=\text{O}$  covalent bond for high laser intensity. Our results show that the intensity-dependent ADIF offers an abundance of dynamics information. This work has directive significance for the further study of strong-field ionization and dissociation dynamics of complex molecules.

#### ACKNOWLEDGMENTS

This work was supported by the National Key Research and Development Program of China (Grant No. 2019YFA0307703), the Major Research plan of National Natural Science Foundation of China (Grant No. 91850201), the NSAF Joint Fund (Grant No. U1830206), and the National Natural Science Foundation of China (Grants No. 11974426, No. 11974425, and No. 11774322).

- [1] A. S. Alnaser, X. M. Tong, T. Osipov, S. Voss, C. M. Maharjan, P. Ranitovic, B. Ulrich, B. Shan, Z. Chang, C. D. Lin, and C. L. Cocke, *Phys. Rev. Lett.* **93**, 183202 (2004).
- [2] E. Baldit, S. Saugout, and C. Cornaggia, *Phys. Rev. A* **71**, 021403(R) (2005).
- [3] M. Pitzer, M. Kunitski, A. S. Johnson, T. Jahnke, H. Sann, F. Sturm, L. P. H. Schmidt, H. Schmidt-Böcking, R. Dörner, J. Stohner, J. Kiedrowski, M. Reggelin, S. Marquardt, A. Schießler, R. Berger, and M. S. Schöffler, *Science* **341**, 1096 (2013).
- [4] A. Méry, V. Kumar, X. Fléchar, B. Gervais, S. Guillous, M. Lalande, J. Rangama, W. Wolff, and A. Cassimi, *Phys. Rev. A* **103**, 042813 (2021).
- [5] C. Ellert and P. B. Corkum, *Phys. Rev. A* **59**, R3170 (1999).
- [6] P. Dietrich, D. T. Strickland, M. Laberge, and P. B. Corkum, *Phys. Rev. A* **47**, 2305 (1993).
- [7] S. Voss, A. S. Alnaser, X. M. Tong, C. Maharjan, P. Ranitovic, B. Ulrich, B. Shan, Z. Chang, C. D. Lin, and C. L. Cocke, *J. Phys. B: At. Mol. Opt. Phys.* **37**, 4239 (2004).
- [8] A. S. Alnaser, C. M. Maharjan, X. M. Tong, B. Ulrich, P. Ranitovic, B. Shan, Z. Chang, C. D. Lin, C. L. Cocke, and I. V. Litvinyuk, *Phys. Rev. A* **71**, 031403(R) (2005).
- [9] X. M. Tong, Z. X. Zhao, and C. D. Lin, *Phys. Rev. A* **66**, 033402 (2002).
- [10] Z. X. Zhao, X. M. Tong, and C. D. Lin, *Phys. Rev. A* **67**, 043404 (2003).
- [11] A. S. Alnaser, S. Voss, X. M. Tong, C. M. Maharjan, P. Ranitovic, B. Ulrich, T. Osipov, B. Shan, Z. Chang, and C. L. Cocke, *Phys. Rev. Lett.* **93**, 113003 (2004).
- [12] X. M. Tong, Z. X. Zhao, A. S. Alnaser, S. Voss, C. L. Cocke, and C. D. Lin, *J. Phys. B: At. Mol. Opt. Phys.* **38**, 333 (2005).
- [13] H. Stapelfeldt and T. Seideman, *Rev. Mod. Phys.* **75**, 543 (2003).
- [14] J. H. Posthumus, J. Plumridge, M. K. Thomas, K. Codling, L. J. Frasinski, A. J. Langley, and P. F. Taday, *J. Phys. B: At. Mol. Opt. Phys.* **31**, L553 (1998).
- [15] X. Ding, M. Haertelt, S. Schlauderer, M. S. Schuurman, A. Y. Naumov, D. M. Villeneuve, A. R. W. McKellar, P. B. Corkum, and A. Staudte, *Phys. Rev. Lett.* **118**, 153001 (2017).
- [16] X. Xie, C. Wu, Y. Liu, W. Huang, Y. Deng, Y. Liu, Q. Gong, and C. Wu, *Phys. Rev. A* **90**, 033411 (2014).
- [17] T. Seideman, M. Y. Ivanov, and P. B. Corkum, *Phys. Rev. Lett.* **75**, 2819 (1995).
- [18] J. Wu, M. Meckel, L. Schmidt, M. Kunitski, S. Voss, H. Sann, H. Kim, T. Jahnke, A. Czasch, and R. Dörner, *Nat. Commun.* **3**, 1113 (2012).
- [19] K. Schnorr, A. Senftleben, M. Kurka, A. Rudenko, L. Foucar, G. Schmid, A. Broska, T. Pfeifer, K. Meyer, D. Anielski, R. Boll, D. Rolles, M. Kübel, M. F. Kling, Y. H. Jiang, S. Mondal, T. Tachibana, K. Ueda, T. Marchenko, M. Simon *et al.*, *Phys. Rev. Lett.* **111**, 093402 (2013).
- [20] H.-K. Kim, H. Gassert, M. S. Schöffler, J. N. Titze, M. Waitz, J. Voigtsberger, F. Trinter, J. Becht, A. Kalinin, N. Neumann, C. Zhou, L. P. H. Schmidt, O. Jagutzki, A. Czasch, H. Merabet, H. Schmidt-Böcking, T. Jahnke, A. Cassimi, and R. Dörner, *Phys. Rev. A* **88**, 042707 (2013).
- [21] T. Jahnke, H. Sann, T. Havermeier, K. Kreidi, C. Stuck, M. Meckel, M. Schöffler, N. Neumann, R. Wallauer, S. Voss, A. Czasch, O. Jagutzki, A. Malakzadeh, F. Afaneh, T. Weber, H. Schmidt-Böcking, and R. Dörner, *Nat. Phys.* **6**, 139 (2010).
- [22] J. Matsumoto, A. Leredde, X. Flechard, K. Hayakawa, H. Shiromaru, J. Rangama, C. L. Zhou, S. Guillous, D. Hennecart, T. Muranaka, A. Mery, B. Gervais, and A. Cassimi, *Phys. Rev. Lett.* **105**, 263202 (2010).
- [23] X. Ren, E. Jabbour Al Maalouf, A. Dorn, and S. Denifl, *Nat. Commun.* **7**, 11093 (2016).
- [24] Q. Cheng, X. Xie, Z. Yuan, X. Zhong, Y. Liu, Q. Gong, and C. Wu, *J. Phys. Chem. A* **121**, 3891 (2017).
- [25] Y. L. Wang, X. Y. Lai, S. G. Yu, R. P. Sun, X. J. Liu, M. Dorner-Kirchner, S. Erattupuzha, S. Larimian, M. Koch, V. Hanus, S. Kangaparambil, G. Paulus, A. Baltuška, X. Xie, and M. Kitzler-Zeiler, *Phys. Rev. Lett.* **125**, 063202 (2020).
- [26] J. Wu, X. Gong, M. Kunitski, F. K. Amankona-Diawuo, L. P. H. Schmidt, T. Jahnke, A. Czasch, T. Seideman, and R. Dörner, *Phys. Rev. Lett.* **111**, 083003 (2013).
- [27] P. Song, X. Wang, C. Meng, W. Dong, Y. Li, Z. Lv, D. Zhang, Z. Zhao, and J. Yuan, *Phys. Rev. A* **99**, 053427 (2019).
- [28] X. Gong, M. Kunitski, L. P. H. Schmidt, T. Jahnke, A. Czasch, R. Dörner, and J. Wu, *Phys. Rev. A* **88**, 013422 (2013).
- [29] W. Quan, V. V. Serov, M. Z. Wei, M. Zhao, Y. Zhou, Y. L. Wang, X. Y. Lai, A. S. Kheifets, and X. J. Liu, *Phys. Rev. Lett.* **123**, 223204 (2019).
- [30] M. Dehghany, A. McKellar, M. Afshari, and N. Moazzen-Ahmadi, *Mol. Phys.* **108**, 2195 (2010).
- [31] A. Schriver, L. Schriver-Mazuoli, and A. A. Vigasin, *Vib. Spectrosc.* **23**, 83 (2000).
- [32] K. W. Jucks, Z. S. Huang, D. Dayton, R. E. Miller, and W. J. Lafferty, *J. Chem. Phys.* **86**, 4341 (1987).
- [33] K. W. Jucks, Z. S. Huang, R. E. Miller, G. T. Fraser, A. S. Pine, and W. J. Lafferty, *J. Chem. Phys.* **88**, 2185 (1988).
- [34] J. Ullrich, R. Moshhammer, A. Dorn, R. Dörner, L. P. H. Schmidt, and H. Schmidt-Böcking, *Rep. Prog. Phys.* **66**, 1463 (2003).
- [35] J. Ullrich, R. Moshhammer, R. Dörner, O. Jagutzki, V. Mergel, H. Schmidt-Böcking, and L. Spielberger, *J. Phys. B: At. Mol. Opt. Phys.* **30**, 2917 (1997).
- [36] R. Dörner, V. Mergel, O. Jagutzki, L. Spielberger, J. Ullrich, R. Moshhammer, and H. Schmidt-Böcking, *Phys. Rep.* **330**, 95 (2000).
- [37] W. Iskandar, A. S. Gattton, B. Gaire, F. P. Sturm, K. A. Larsen, E. G. Champenois, N. Shivaram, A. Moradmand, J. B. Williams, B. Berry, T. Severt, I. Ben-Itzhak, D. Metz, H. Sann, M. Weller, M. Schoeffler, T. Jahnke, R. Dörner, D. Slaughter, and T. Weber, *Phys. Rev. A* **99**, 043414 (2019).
- [38] B. Manschwetus, H. Rottke, G. Steinmeyer, L. Foucar, A. Czasch, H. Schmidt-Böcking, and W. Sandner, *Phys. Rev. A* **82**, 013413 (2010).
- [39] W. Iskandar, J. Matsumoto, A. Leredde, X. Fléchar, B. Gervais, S. Guillous, D. Hennecart, A. Méry, J. Rangama, C. L. Zhou, H. Shiromaru, and A. Cassimi, *Phys. Rev. Lett.* **114**, 033201 (2015).
- [40] Y. Sato, H. Kono, S. Koseki, and Y. Fujimura, *J. Am. Chem. Soc.* **125**, 8019 (2003).
- [41] B. Walker, B. Sheehy, L. F. DiMauro, P. Agostini, K. J. Schafer, and K. C. Kulander, *Phys. Rev. Lett.* **73**, 1227 (1994).
- [42] C. Cornaggia and P. Hering, *Phys. Rev. A* **62**, 023403 (2000).
- [43] C. Guo, M. Li, J. P. Nibarger, and G. N. Gibson, *Phys. Rev. A* **61**, 033413 (2000).



- [44] B. Ulrich, A. Vredenburg, A. Malakzadeh, M. Meckel, K. Cole, M. Smolarski, Z. Chang, T. Jahnke, and R. Dörner, *Phys. Rev. A* **82**, 013412 (2010).
- [45] T. Weber, M. Weckenbrock, A. Staudte, L. Spielberger, O. Jagutzki, V. Mergel, F. Afaneh, G. Urbasch, M. Vollmer, H. Giessen, and R. Dörner, *Phys. Rev. Lett.* **84**, 443 (2000).
- [46] T. Zuo and A. D. Bandrauk, *Phys. Rev. A* **52**, R2511 (1995).
- [47] G. N. Gibson, R. N. Coffee, and L. Fang, *Phys. Rev. A* **73**, 023418 (2006).
- [48] A. Saenz, *Phys. Rev. A* **61**, 051402(R) (2000).
- [49] G. N. Gibson, R. R. Freeman, and T. J. McIlrath, *Phys. Rev. Lett.* **67**, 1230 (1991).
- [50] D. Dimitrovski, C. P. J. Martiny, and L. B. Madsen, *Phys. Rev. A* **82**, 053404 (2010).
- [51] D. Pavičić, K. F. Lee, D. M. Rayner, P. B. Corkum, and D. M. Villeneuve, *Phys. Rev. Lett.* **98**, 243001 (2007).
- [52] Y. Huang, C. Meng, X. Wang, Z. Lü, D. Zhang, W. Chen, J. Zhao, J. Yuan, and Z. Zhao, *Phys. Rev. Lett.* **115**, 123002 (2015).
- [53] I. Thomann, R. Lock, V. Sharma, E. Gagnon, S. T. Pratt, H. C. Kapteyn, M. M. Murnane, and W. Li, *J. Phys. Chem. A* **112**, 9382 (2008).
- [54] I. V. Litvinyuk, K. F. Lee, P. W. Dooley, D. M. Rayner, D. M. Villeneuve, and P. B. Corkum, *Phys. Rev. Lett.* **90**, 233003 (2003).
- [55] D. Pinkham and R. R. Jones, *Phys. Rev. A* **72**, 023418 (2005).
- [56] J. Wu, L. P. H. Schmidt, M. Kunitski, M. Meckel, S. Voss, H. Sann, H. Kim, T. Jahnke, A. Czasch, and R. Dörner, *Phys. Rev. Lett.* **108**, 183001 (2012).
- [57] H. Akagi, T. Otobe, A. Staudte, A. Shiner, F. Turner, R. Dörner, D. M. Villeneuve, and P. B. Corkum, *Science* **325**, 1364 (2009).
- [58] B. K. McFarland, J. P. Farrell, P. H. Bucksbaum, and M. Guhr, *Science* **322**, 1232 (2008).
- [59] O. Smirnova, Y. Mairesse, S. Patchkovskii, N. Dudovich, D. Villeneuve, P. Corkum, and M. Y. Ivanov, *Nature (London)* **460**, 972 (2009).
- [60] S. Haessler, J. Caillat, W. Boutu, C. Giovanetti-Teixeira, T. Ruchon, T. Auguste, Z. Diveki, P. Breger, A. Maquet, B. Carré, R. Taleb, and P. Salières, *Nat. Phys.* **6**, 200 (2010).
- [61] A. Castro, H. Appel, M. Oliveira, C. A. Rozzi, X. Andrade, F. Lorenzen, M. A. L. Marques, E. K. U. Gross, and A. Rubio, *Phys. Status Solidi B* **243**, 2465 (2006).
- [62] S.-K. Son and S.-I. Chu, *Phys. Rev. A* **80**, 011403(R) (2009).
- [63] C. Ullrich, *J. Mol. Struct. (THEOCHEM)* **501-502**, 315 (2000).